Effect of Strain Rate on Damage Evolution in a Cast Al-Si-Mg Base Alloy

MANISH D. DIGHE, ARUN M. GOKHALE, MARK F. HORSTEMEYER, and D.A. MOSHER

An important aspect of damage evolution in cast Al-Si-Mg base alloys is fracture/cracking of Si particles. This microstructural damage is quantitatively characterized as a function of strain rate in the range 10^{-4} to $3.7 \times 10^{+3}$, at an approximately constant uniaxial compressive strain level (20 to 25 pct). It is shown that the fraction of damaged silicon particles, their average size, and size distribution do not vary significantly with the strain rate, and at all strain rates studied, larger Si particles are more likely to crack than the smaller ones. However, the stress-strain curves *are* sensitive to the strain rate. These observations have implications for modeling of deformation and fracture of cast components under high strain rate crash conditions.

I. INTRODUCTION

THE A356 and other Al-Si-Mg base cast alloys are widely used for automotive structural applications. Mechanical properties and fracture behavior of these cast alloys depend on macrodefects such as internal oxide layers and shrinkage macroporosity,[1,2] microporosity,[3,4] dendritic cell size,[5,6] and size and shape of silicon particles[7] present in the interdendritic regions. Fracture and debonding of silicon particles is an important aspect of damage evolution in these alloys.[3,7–9] Fracturing of silicon particles, formation and growth of voids around silicon particles, and subsequent interlinkage of the voids leads to crack propagation in the interdendritic regions. Figure 1 illustrates this fracture micro mechanism. It is observed that silicon particles fracture at stresses significantly below the ultimate tensile strength, but almost always above yield strength of the material.[7] There have been numerous studies on the fraction of damaged silicon particles in Al-Si-Mg alloys.[7,10,11] Recently, the effect of temperature on fraction of damaged Si particles in A356 alloy has been reported.[12] However, in all the earlier investigations, the mechanical tests were performed at a fixed low strain rate (typically of the order of 10^{-4} or so), and therefore, no quantitative data are available on the effect of strain rate on microstructural damage in Al-Si-Mg based alloys.[1] Under crash conditions, structural automobile components are likely to experience high strain rates (on the order of 1 to 100). Therefore, it is of interest to study the effect of strain rate on the Si particle damage. Such quantitative microstructural damage evolution data are also required for modeling deformation and fracture of cast automotive components under crash conditions.[13] It is the purpose of this contribution to report experimental observations on the effect of strain rate on fraction of damaged Si particles in a chill cast A356 alloy (which is a typical Al-Si-Mg base cast alloy) under compression. The experiments were performed at strain rates ranging from 10^{-4} to 4.9×10^{3} (*i.e.*, variation of over seven orders of magnitudes) in order to characterize the strain rate dependence of the damage.*

*To the best of our knowledge, quantitative microstructural data concerning the effect of strain rate on damage development are not available in any alloy system.

MANISH D. DIGHE, Graduate Student, and ARUN M. GOKHALE, Professor, are with the School of Materials Science and Engineering, Georgia Institute of Technology, Atlanta, GA 30332-0245. MARK F. HORSTEMEYER, Principal Member of the Technical Staff, is with the Center for Materials and Engineering Sciences, Livermore, CA 94550. D.A. MOSHER, Research Engineer, is with United Technologies Research Center, East Hartford, CT 06108.

Manuscript submitted January 12, 1999.

II. EXPERIMENTAL WORK

A. *Material and Heat Treatment*

Experiments were performed on a commercial A356 alloy (7 pct Si, 0.4 pct Mg). A rectangular plate casting of dimensions $203.2 \times 139.7 \times 25.4$ mm was made by using iron chills on top, bottom, and side opposite to the riser end of the plate to simulate a permanent mold casting. A no bake silica sand was used for the riser and down sprue. A ceramic filter was placed between the riser and the down sprue. The melt was grain refined, strontium modified, and degassed using a rotary degasser. The liquid metal was poured at temperature in the range of 950 to 977 K. The castings were cooled for a period of about 16 hours and then removed from the molds. The cast plates were solution treated at 810 K for 16 hours, hot water quenched at 344 K, and then artificially aged at 492 K for 4 hours, to achieve T6 temper. Compression test specimens were machined from the low porosity (<0.1 pct) regions of the cast plates near the chill end.

B. *Mechanical Tests*

1. *Low strain rate compression tests*

The compression test specimens were designed to produce homogeneous deformation throughout the specimen by introducing grooves that were machined into specimen ends.[14] Lubrication was placed into the grooves to alleviate frictional forces to avoid barreling of the specimen.[15] The low strain rate compression tests were performed at Westmoreland Mechanical Testing and Research Laboratory (Pennsylvania). The tests were conducted at strain rates of 10^{-4}, 10^{-2}, and 1 per second at room temperature under displacement control in a servohydraulic Instron test frame.

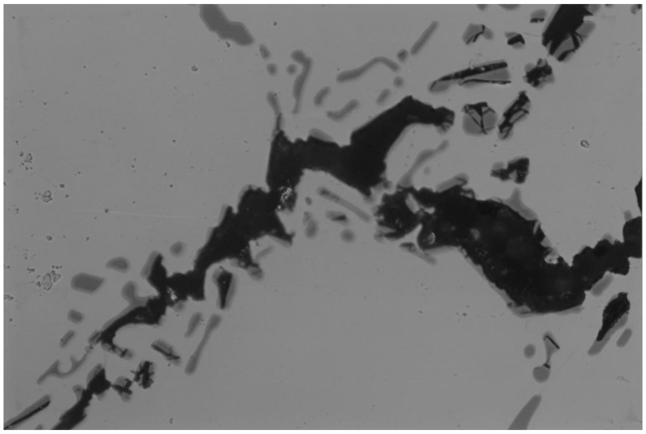

Fig. 1—Fracture of Si particles, void growth, coalescence, and interlinkage of cracks in interdendritic eutectic lead to the global fracture.

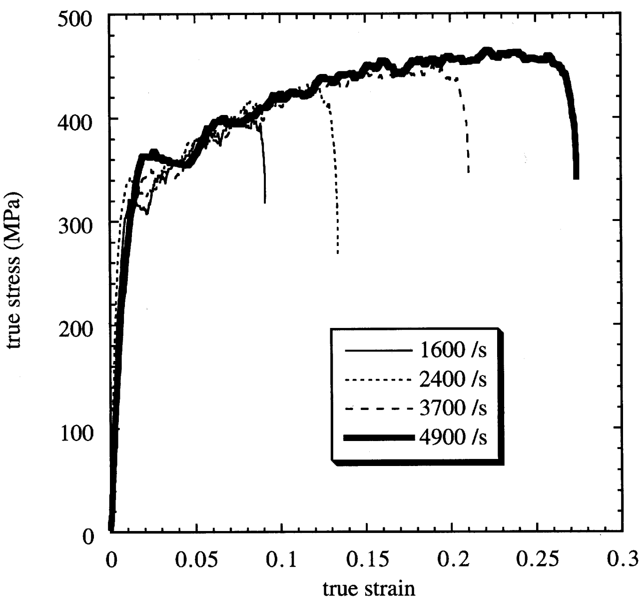

Fig. 2—Strain-strain response at high strain rates.

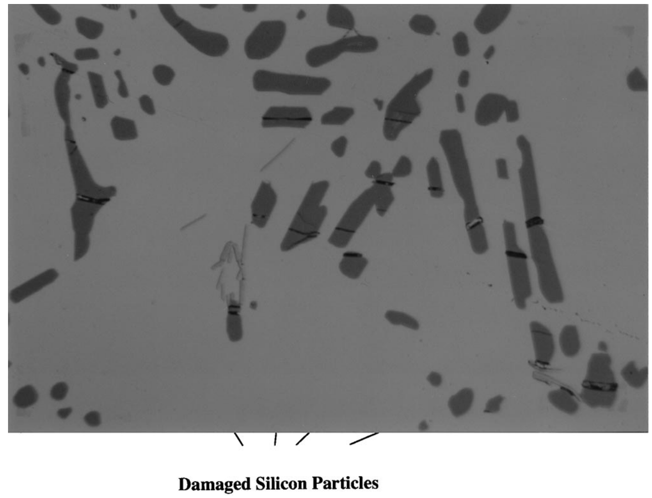

Fig. 3—Si particle damage under compressive load.

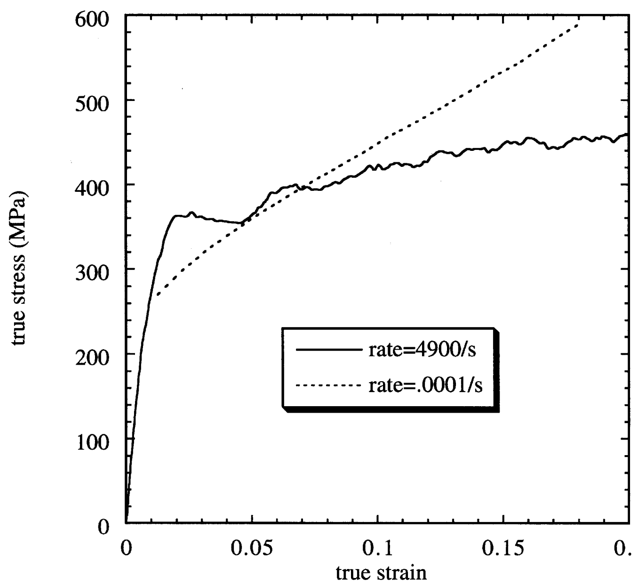

Fig. 4—Comparison of stress-strain curves for compression tests performed at lowest (10^{-4}) and highest (3.7×10^3) strain rates.

The quasi-static tests were interrupted at 20 to 25 pct compression strain. In addition, interrupted compressive tests were carried to study the damage evolution of silicon particles at the same strain rate. The strain levels chosen were 0.1, 0.5, 1, 2, and 5 pct, and the strain rate used was 10^{-4}.

2. *High strain rate tests*

The high strain rate tests were performed at Sandia National Laboratory on a compressive split Hopkinson bar system.[16] These specimens had length to diameter ratio of 0.5 to reduce wave reverberation time and radial inertia effects. The specimens were ungrooved and they were lubricated with MoS_2 grease. The tested specimens had rough surface (orange peel effect) at both ends, which is an important indicator of uniform deformation in the specimen. Figure 2 shows stress-strain response of some high strain rate Hopkinson bar test specimens.

3. *Tension tests*

To quantify the differences in the damage evolution under tensile and compressive loads, tensile tests were performed at the strain rate of 10^{-4}. Specimens were tested up to various tensile strain levels. The strain levels chosen were 0.3, 0.7, 1.0, 2.0, 5.0, and 7.5 pct (fracture strain). Tensile tests were not performed at any other strain rates.

C. *Quantitative Metallography*

The fractured specimens were cut in the center along a vertical plane containing the applied load direction, and they were polished by using standard metallographic procedures. Figure 3 illustrates the microstructures revealed in this manner. Observe that the fractured silicon particles are present in the specimens tested at both the highest and the lowest strain rates. To quantify this microstructural damage, about 200 fields of view were analyzed in each specimen at a magnification of 500 times. In each field of view, number of damaged silicon particles were counted manually, and total number of silicon particles were counted by using

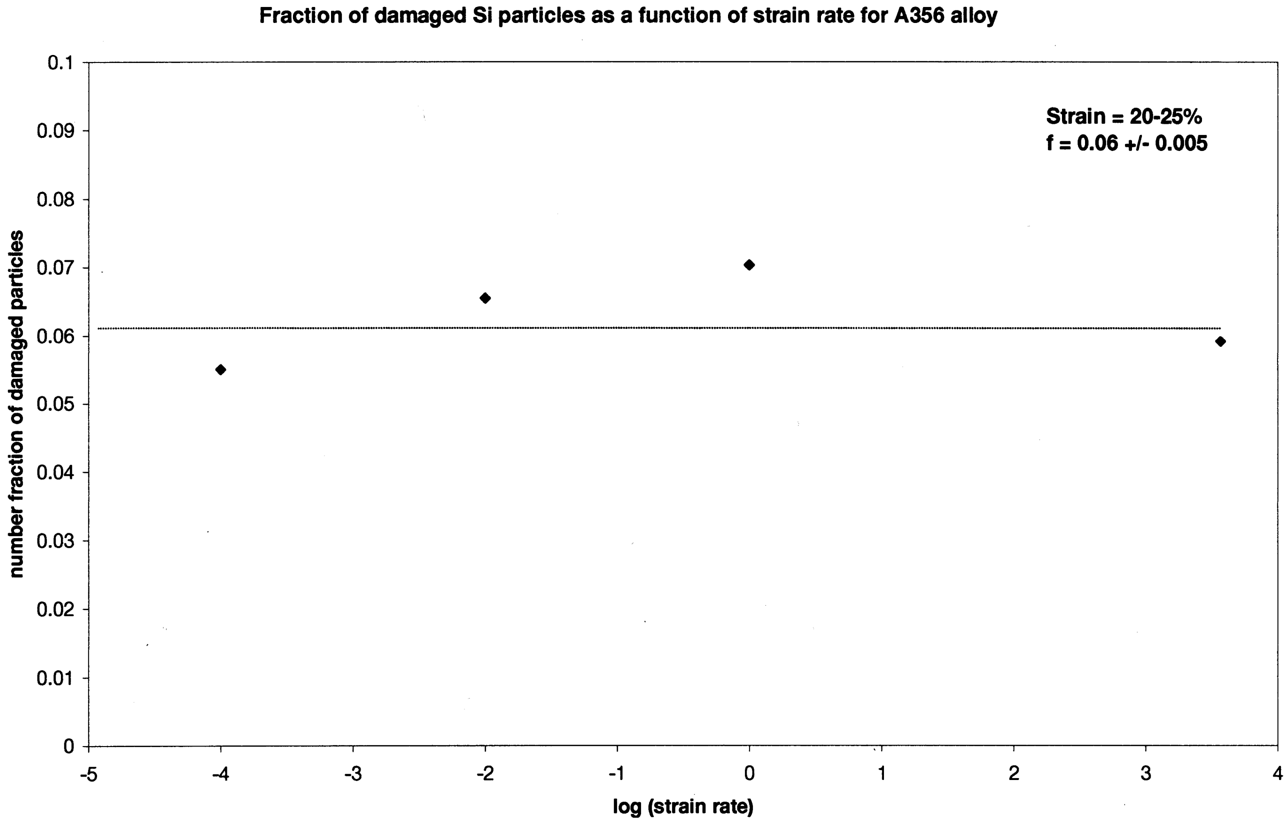

Fig. 5—Variation of number fraction of damaged Si particles with the strain rate.

automatic digital image analysis. In addition, the size* of each silicon particle was measured by using field specific digital image analysis, and the total area fraction of all the damaged silicon particles was measured by using field specific digital image analysis. From these measurements, the number fraction, area fraction, and size distribution of damaged silicon particles were calculated.

*In this study, longest characteristic dimension of Si particles is used to characterize their size.

III. RESULTS AND DISCUSSION

Figure 4 shows true stress-strain curves for compression tests performed at the low (10^{-4} per second) and high (4.9×10^3 per second) curves. These data reveal the effect of strain rate on yield stress and hardening rate. The yield stress is significantly lower at lower strain rates, whereas the work hardening rate is significantly higher. Note that at low strain rates, the deformation is isothermal, but at high strain rates, it is essentially adiabatic. This is because at high strain rates, there is not sufficient time for heat dissipation from the specimen. The higher specimen temperature at high strain rates leads to a decrease in the work hardening rate. On the other hand, in this alloy, the dynamic yield point is higher at higher strain rates (as in most alloys), due to lower rate of dislocation generation at higher strain rates. The net result of these two effects is that the flow stress at 10^{-4} strain rate is higher than that at 4.9×10^3 strain rate at higher compressive strains, although the yield stress at 10^{-4} strain rate is lower.

Figure 5 shows a plot of number fraction of damaged Si particles *vs* strain rate. In all of these specimens, the uniaxial compressive strain is approximately the same (about 22 to 25 pct). Thus, at constant strain, there is no statistically significant variation in the number fraction of damaged silicon particles with strain rate, although strain rate is varied by more than seven orders of magnitude. Figure 6 shows the plot of the volume fraction of damaged silicon particles *vs* the strain rate, which shows the trend very similar to that of the number fraction of damaged particles: there is no significant change in the volume fraction of damaged silicon particles with strain rate. Figures 7(a) and (b) show the size distributions of damaged particles at 3.7×10^3 and 10^{-4} strain rates, respectively, and Figure 7(c) depicts overall size distribution of undamaged and damaged silicon particles. Observe that there is no significant difference between the size distribution of damaged Si particles at 3.7×10^3 and 10^{-4} strain rates, but both of these distributions differ very significantly from the overall size distribution of silicon particles shown in Figure 7(c). The average size of the overall size distribution of silicon particles (which includes undamaged and damaged silicon particles) is 6.2 μm, whereas the average size of damaged silicon particles is about 13 to 15 μm. Further, all the damaged silicon particles have sizes larger than the overall average size of silicon particles. This clearly demonstrates that at both high and low strain rates, larger silicon particles are significantly more

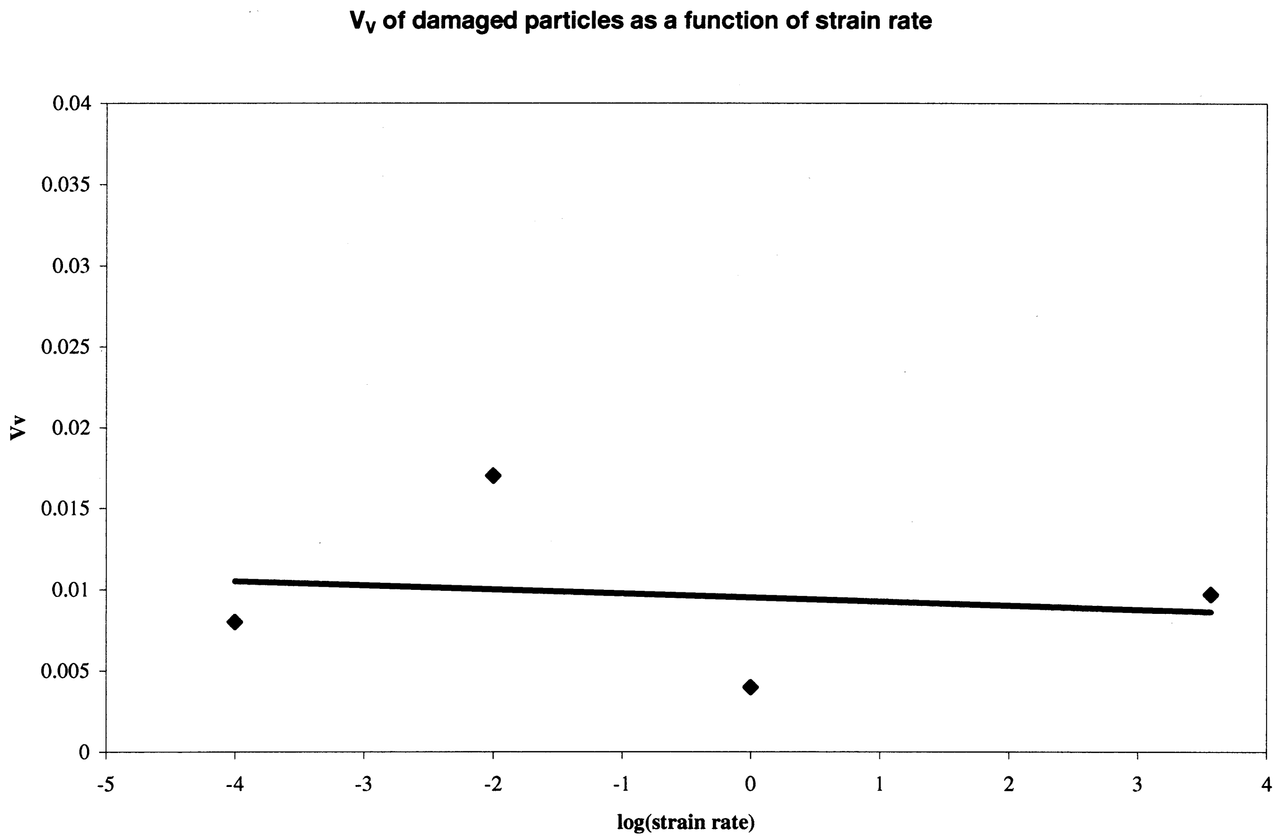

Fig. 6—Variation of volume fraction of damaged Si particles with the strain rate.

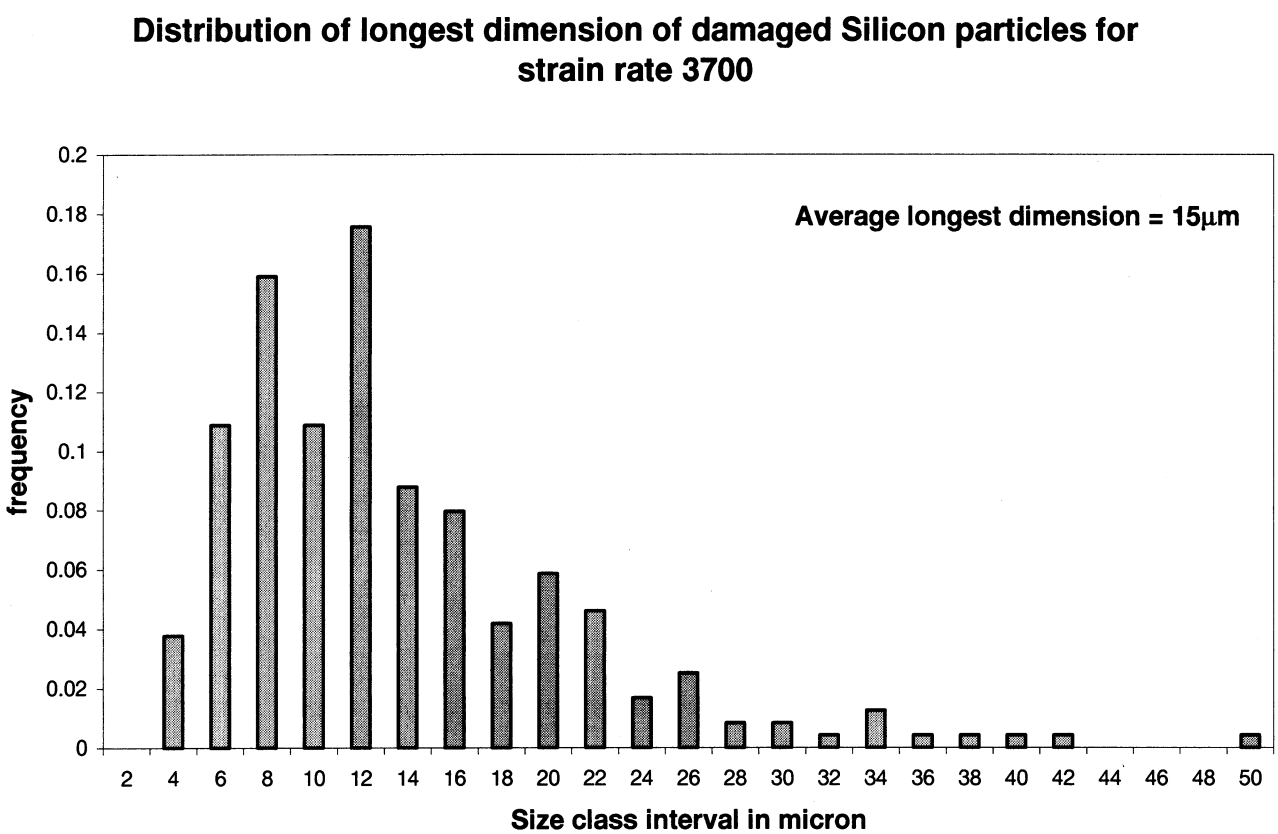

(*a*)

Fig. 7—(*a*) Size distribution of damaged Si particles at 3.7 × 10^3 strain rate. Continued.

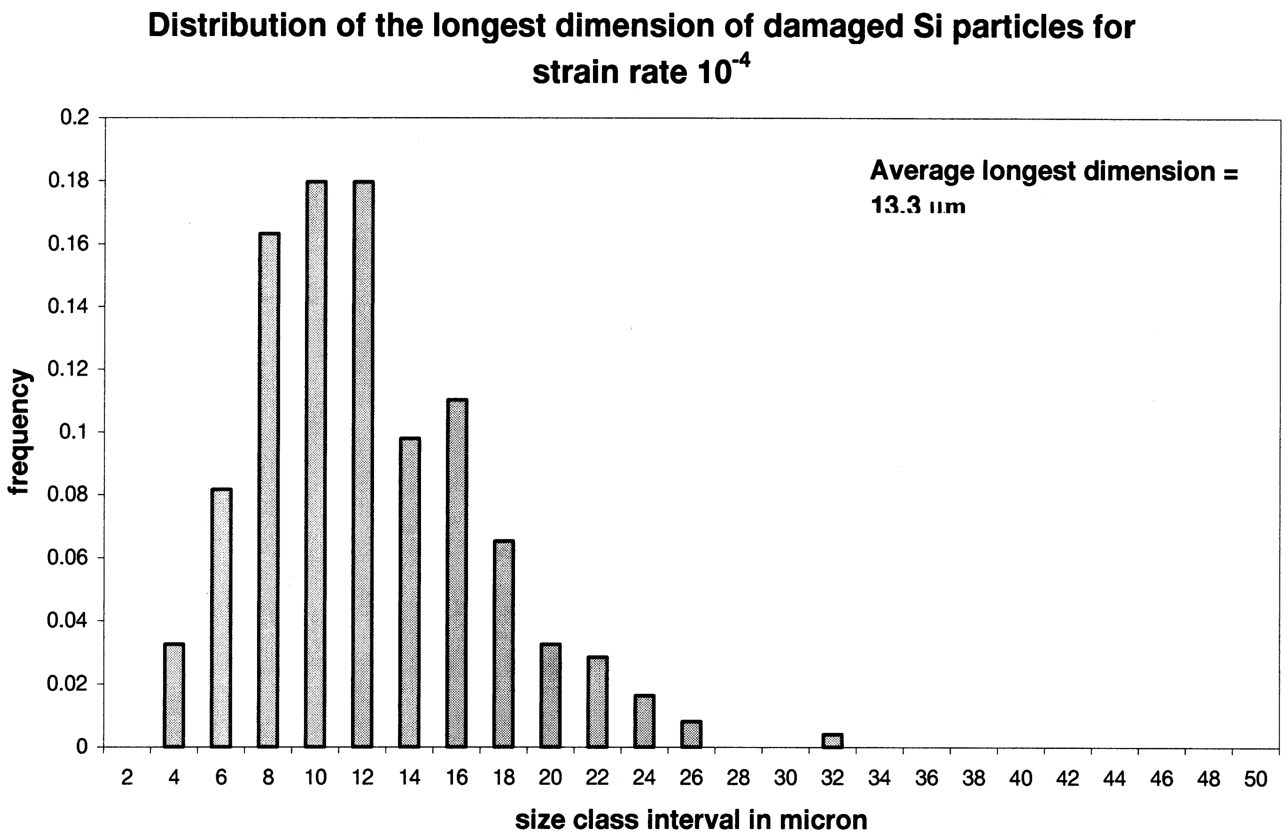

(*b*)

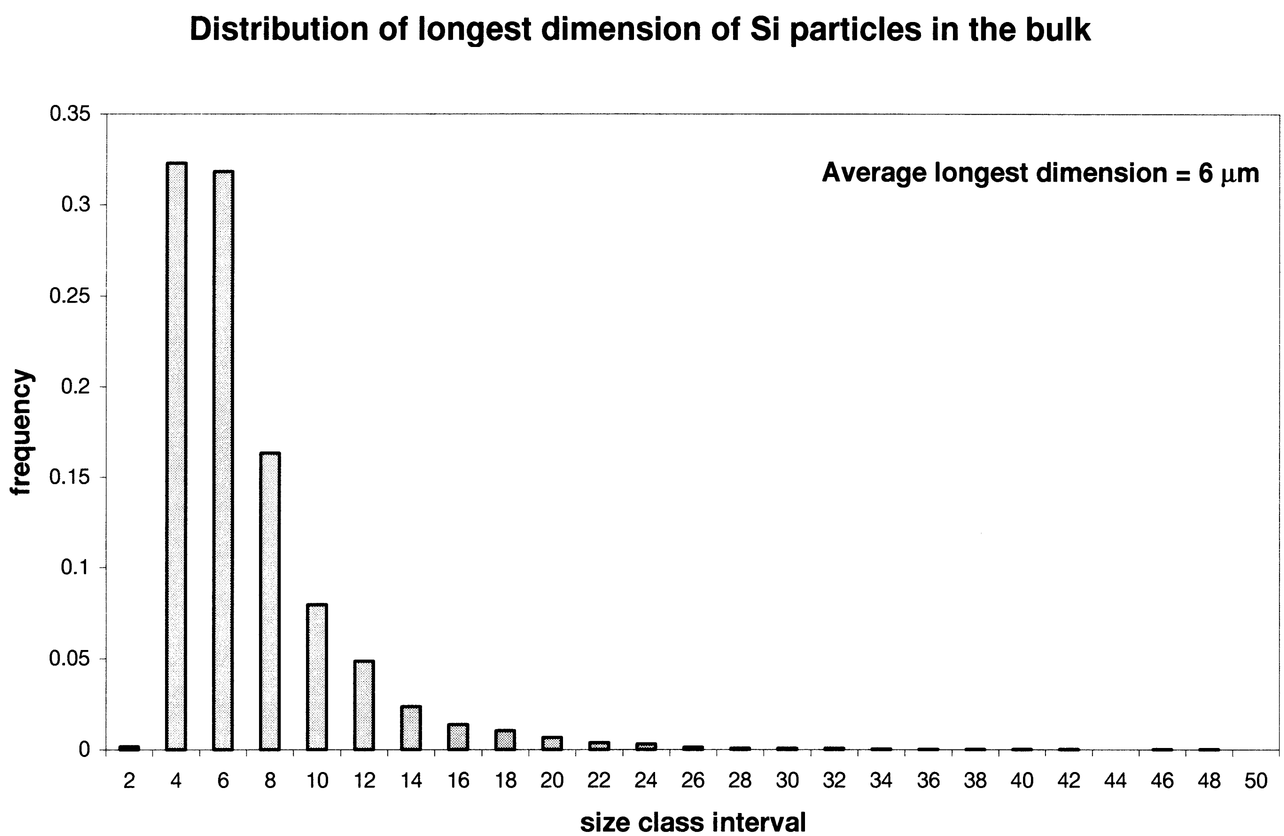

(*c*)

Fig. 7—Continued. (*b*) Size distribution of damaged Si particles at 10^{-4} strain rate. (*c*) Overall size distribution of undamaged and damaged Si particles.

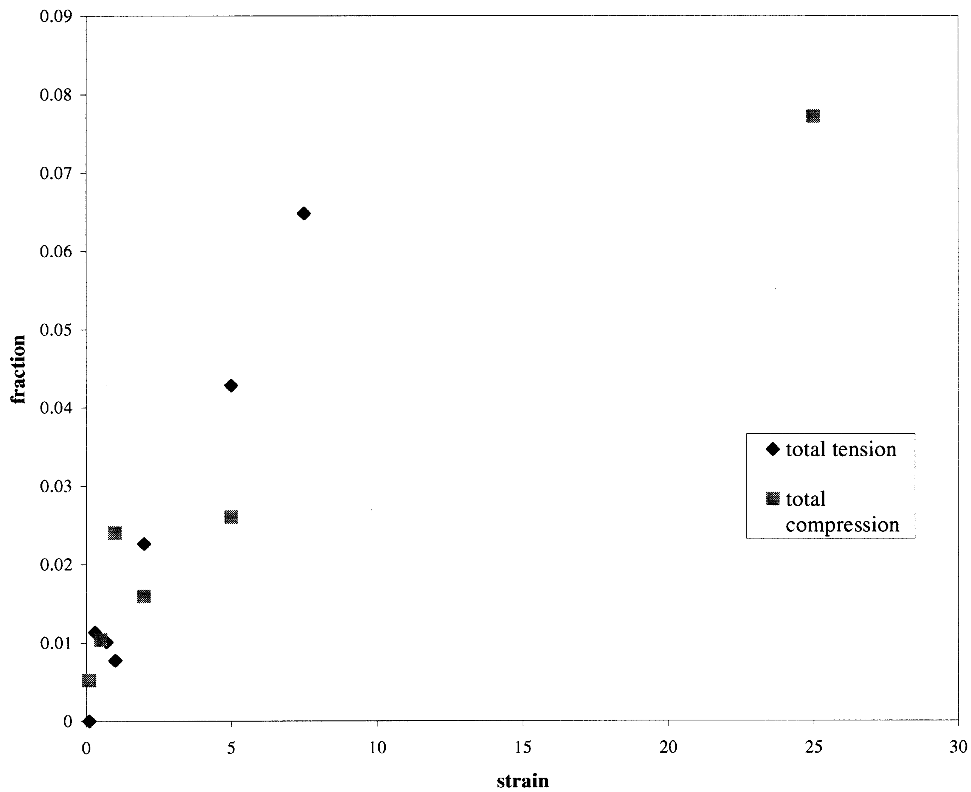

Fig. 8—Variation of number fraction of damaged Si particles with strain under tension and compression at the strain rate of 10^{-4}.

likely to fracture than smaller ones. Therefore, a microstructure consisting of finer average silicon particle size and narrow size distribution (*i.e.*, low variance) is likely to increase fracture resistance of cast A356 alloy components under normal strain rates as well as under crash conditions, where high strain rates are encountered. The present data reveal that, at high compression strain levels (20 to 25 pct), the fraction of damaged silicon particles, the average size of the damaged particles, and their size distribution are not sensitive to the strain rate, at least in the strain rate regime (10^{-4} to 3.7×10^3) studied in this investigation. Under vehicle crash conditions, components experience large strains at relatively high strain rates. Therefore, the damage mechanics and micromechanics based models for silicon particles damage evolution, developed for low strain rate behavior, may also be applicable to describe the damage evolution at relatively high strain rates under crash conditions.

The damage evolution often depends on stress-state and loading condition. Therefore, it is of interest to compare the damage evolution in compression and tension. Figure 8 shows the plot of fraction of damaged silicon particles as a function of strain for uniaxial tension and compression specimens strained at the rate of 10^{-4}. Observe that at a given strain level, the fraction of damaged particles is higher under tension as compared to that under compression.

IV. SUMMARY AND CONCLUSIONS

The experimental data reveal that, at least at high strain levels, the microstructural damage to Si particles in A356 alloy is insensitive to strain rate. On the other hand, the stress-strain behavior under compression is quite sensitive to strain rate; the increase in the strain rate increases the dynamic yield point and decreases the work hardening rate of the alloy.

ACKNOWLEDGMENTS

Authors thank Richard Osborne (General Motors Corp.) and Srinath Vishwanathan (Oak Ridge National Laboratory) for numerous useful discussions and suggestions, G.A. Shulke (Chrysler Corporation) for casting and heat treatment of A356 cast plates. Research at Georgia Tech (MDD and AMG) was supported by research grants from American Foundrymen Society and U.S. National Science Foundation (Grant No. DMR-9816618). The research at Sandia National Laboratory (MFF and DAM) has been sponsored by United States Department of Energy under Contract No. DE-AC04-94AL85000. The financial support is gratefully acknowledged.

REFERENCES

1. M.J. Couper, A.E. Neeson, and J.R. Grifiths: *Fatigue Fract. Eng. Mater.*, 1990, vol. 13 (3), pp. 213-27.
2. M.K. Surappa, E. Blank, and J.C. Jaquet: *Scripta Metall.*, 1986, vol. 20, pp. 1281-86.
3. A.M. Samuel and F.H. Samuel: *Metall. Mater. Trans. A*, 1995, vol. 26A, pp. 2359-72.
4. E.N. Pan, C.S. Lin, and C.R. Roper: *Am. Foundrymen Soc. Trans.*, 1990, vol. 98, pp. 735-46.

5. R.E. Spear and G.R. Gardener: *Am. Foundrymen Soc. Trans.*, 1963, vol. 71, pp. 209-15.
6. J.F. Major, A. Makinde, P.D. Lee, B. Chamberlain, T. Scappaticci, and D. Rickman: *Int. Cong. Exp. on Vehicle Suspension System Advancement*, Detroit, MI, 1994, pp. 117-28.
7. Jien-Wei Yeh and Wen-Pin Liu: *Metall. Mater. Trans. A*, 1996, vol. 27A, pp. 3558-68.
8. M.D. Dighe and A.M. Gokhale: *Scripta Mater.*, 1997, vol. 37, pp. 1435-40.
9. F.T. Lee, J.F. Major, and F.H. Samuel: *Metall. Mater. Trans. A*, 1995, vol. 26A, pp. 1553-70.
10. A. Gangulee and J. Gurland: *Trans. TMS-AIME*, 1967, vol. 239, pp. 269-72.
11. M.D. Dighe: Master's Dissertation, Georgia Institute of Technology, Atlanta, GA, 1998.
12. M.D. Dighe, A.M. Gokhale, and M.F. Horstemeyer: *Metall. Mater. Trans. A*, 1998, vol. 29A, pp. 905-08.
13. M.F. Horstemayer and A.M. Gokhale: *Int. J. Solids Struct.*, vol. 36, 1999, pp. 5029-55.
14. W.A. Kawahara: *Exp. Tech.*, 1990, March–April, pp. 58-60.
15. S.S. Hecker, M.G. Scout, and D.T. Eash: *Proc. Workshop on Plasticity of Metals at Finite Strains: Theory, Experiment, and Computation*, E.H. Lee and R.L. Mallet, eds., Stanford University, Stanford, CA, 1982, pp. 162-201.
16. U.S. Lindholm and L.M. Yeakley: *High Strain Rate Testing: Tension and Compression*, 1968.